Author/s:
McLeod, VM;Lau, CL;Chiam, MDF;Rupasinghe, TW;Roessner, U;Djouma, E;Boon, WC;Turner, BJ

Title:
Androgen receptor antagonism accelerates disease onset in the SOD1G93A mouse model of amyotrophic lateral sclerosis

Date:
2019-07-01

Citation:
McLeod, V. M., Lau, C. L., Chiam, M. D. F., Rupasinghe, T. W., Roessner, U., Djouma, E., Boon, W. C. & Turner, B. J. (2019). Androgen receptor antagonism accelerates disease onset in the SOD1G93A mouse model of amyotrophic lateral sclerosis. British Journal of Pharmacology, 176 (13), pp.2111-2130. https://doi.org/10.1111/bph.14657.

Persistent Link:
https://hdl.handle.net/11343/285814

Androgen receptor antagonism accelerates disease onset in the SOD1^{G93A} mouse model of amyotrophic lateral sclerosis

Victoria M. McLeod[1], Chew L. Lau[1], Mathew D.F. Chiam[1], Thusitha W. Rupasinghe[2], Ute Roessner[2], Elvan Djouma[3], Wah C. Boon[1], Bradley J. Turner[1,*]

[1]*Florey Institute of Neuroscience and Mental Health, University of Melbourne, Parkville, VIC 3052, Australia.*

[2]*Metabolomics Australia, School of BioSciences, University of Melbourne, VIC 3010 Australia*

[3]*Department of Physiology, Anatomy and Microbiology, La Trobe University, VIC 3086 Australia*

*Corresponding author:

Bradley J. Turner

Florey Institute of Neuroscience and Mental Health

University of Melbourne

30 Royal Parade

Parkville, VIC, Australia, 3052

Tel: +61 3 9035 6521, Fax: +61 3 9035 3107

Email: bradley.turner@florey.edu.au

Running Title: Blocking androgen receptors in SOD1^{G93A} transgenic mice

Author Contributions: BJT conceived the study. BJT, WCB & CLL provided supervision. VMM conducted all mouse efficacy studies, biochemical and histological analysis and interpretation with assistance from MDC. CLL generated hESC-derived motor neurons. TWR and UR performed LC-MS-MS analysis. CLL, WCB and ED assisted in data interpretation. VMM and BJT wrote manuscript with all authors contributing to edits. All authors approved the final version.

Keywords: Androgens, androgen receptor, ALS, SOD1^{G93A} mice, muscle atrophy, motor neurons

ABSTRACT

Background and Purpose: Amyotrophic lateral sclerosis (ALS) is a fatal neurodegenerative disease typically more common in males, implicating androgens in progression of both patients and mouse models. Androgen effects are mediated by the androgen receptor (AR) which is highly expressed in spinal motor neurons and skeletal muscles. To clarify the role of AR in ALS, we therefore examined the effect of AR antagonism in the $SOD1^{G93A}$ mouse model.

Experimental Approach: The androgen receptor antagonist, flutamide, was administered to presymptomatic $SOD1^{G93A}$ mice as a slow-release subcutaneous implant (5 $mg.d^{-1}$). Testosterone, flutamide and metabolite levels were measured in blood and spinal cord tissue by LC-MS-MS. Effects of AR inhibition on disease onset and progression were assessed using motor function tests, survival, muscle and neuropathological analyses.

Key Results: Flutamide was metabolized to 2-hydroxyflutamide achieving steady state plasma levels across the study duration and reached the spinal cord at pharmacologically active concentrations. AR antagonism accelerated disease onset and locomotor dysfunction in male $SOD1^{G93A}$ mice, but not female mice, without affecting survival. Analysis of hindlimb muscles revealed exacerbation in myofibre atrophy of male $SOD1^{G93A}$ mice treated with flutamide, although motor neuron pathology was not affected.

Conclusion and Implications: Our findings suggest AR antagonism accelerates disease onset in male $SOD1^{G93A}$ mice leading to exacerbated muscle pathology, consistent with a role of androgens in modulating disease severity, sexual dimorphism and peripheral pathology in ALS. These results also demonstrate a key contribution of skeletal muscle pathology to disease onset, but not outcome, in this mouse model of ALS.

Abbreviations: ALS, amyotrophic lateral sclerosis; AR, androgen receptor; DHT, dihydrotestosterone; HF, 2-hydroxyflutamide; SBMA, spinal bulbar and muscular atrophy.

INTRODUCTION

Amyotrophic lateral sclerosis (ALS) is a fatal adult onset neurodegenerative disorder characterised by the loss of upper (motor cortex) and lower (brainstem and spinal cord) motor neurons, ultimately resulting in respiratory paralysis and death typically within 3-5 years following diagnosis (Brown & Al-Chalabi, 2017). ALS pathophysiology encompasses both cell and non-cell autonomous mechanisms, the latter involving centrally (astrocytes, microglia and oligodendrocytes) and peripherally (Schwann cells, skeletal myocytes and T-cells) acting contributors to motor neuron survival (Taylor et al., 2016). The origins and trajectory of motor neuron loss within the central nervous system (CNS) has become one of the most contested topics in ALS research. Two main theories have emerged; the "dying-forward" hypothesis which proposes that upper motor neurons initially die, promoting the death of their monosynaptic connections, the lower motor neurons in the spinal cord through glutamate toxicity (Geevasinga et al., 2016); and secondly the "dying-back" hypothesis whereby the disease starts in the lower motor neurons with the destruction of the neuromuscular junction (NMJ) and retraction of axons preceding cell death (Moloney et al., 2014).

ALS shows sexual dimorphism in incidence, age of onset and anatomical site of onset, with males usually having higher incidence, earlier age of onset and presenting with spinal onset symptoms, as opposed to bulbar onset (McCombe & Henderson, 2010). While this evidence is largely based on cohorts of sporadic ALS patients, accounting for 90% of the disease, other evidence suggests a male predominance in familial ALS patients with SOD1 mutations (Kim et al., 2007) and *C9orf72* repeat expansions (Rooney et al., 2017). Sex-effects are recapitulated in the $SOD1^{G93A}$ mouse model of ALS with males showing earlier disease onset with decreased survival, depending on the background strain (Pfohl et al., 2015).

Furthermore, TDP-43^{A315T} male mice have earlier disease onset and death, compared to females (Hatzipetros et al., 2013). Collectively, this evidence implicates hormonal influences, particularly androgens, in ALS pathogenesis.

Androgens, primarily testosterone and dihydrotestosterone (DHT), exert their biological effects through activation of the androgen receptor (AR), a nuclear steroid receptor involved in the regulation of target gene transcription. AR function is important to the survival, growth and maintenance of both skeletal muscle and motor neurons (Cary & La Spada, 2008; Fargo et al., 2008; Rana et al., 2014). Androgens promote neurite outgrowth in cultured motor neurons (Marron et al., 2005) and promote recovery from facial nerve crush injury (Kujawa et al., 1991), as well as spinal and cranial nerve axotomy *in vivo* (Fargo et al., 2008). The polyglutamine disorder, spinal bulbar muscular atrophy (SBMA), arises from a CAG repeat expansion mutation in the *AR* gene and leads to selective lower motor neuron death (Beitel et al., 2013; La Spada et al., 1991), underscoring the importance of AR signalling for motor neuron health.

The role of androgens in ALS, whether detrimental or protective, remains unclear however. Castration of male SOD1^{G93A} mice to deplete circulating androgens does not modify disease onset or survival (Aggaarwal et al., 2014; Sheean et al., 2015), most likely due to persisting androgen production from adrenal glands, arguing for more systemic approaches to block AR signalling. In male SOD1^{G93A} mice, administration of DHT was neuroprotective and improved survival (Yoo & Ko, 2012), while conversely treatment with the anabolic steroid nandrolone worsened the phenotype in castrated SOD1^{G93A} mice (Aggarwal et al., 2014). However, there have been no studies of the effects of anti-androgens in ALS to date.

Here, we examine the effects of flutamide treatment on disease onset, progression and pathology in SOD1^{G93A} mice. Flutamide is classified as a first-generation nonsteroidal antiandrogen therapy primarily used in the treatment of prostate cancer. Its mechanism of action as a competitive androgen receptor antagonist, negates the effects mediated by testosterone and DHT. Flutamide is a small molecule drug well absorbed following oral and subcutaneous administration and is rapidly metabolised by the liver CYP1A2 enzyme (Matsuzaki et al., 2006) to its biologically active form, 2-hydroxyflutamide (HF). Here, flutamide administered to presymptomatic SOD1^{G93A} mice accelerated onset of disease and locomotor deficits in males, but not females, without affecting survival. In concert, flutamide worsened muscle atrophy at gene expression and histological levels in treated male SOD1^{G93A} mice, suggesting impaired AR signalling is detrimental in ALS.

METHODS

Ethical statement

All animal experimentation was conducted in accordance with the Australian National Health and Medical Research Council published Code of Practice and was approved by the Florey Institute of Neuroscience and Mental Health Animal Ethics Committee (approval number 15-060-FINMH). Animal work is reported in accordance with the ARRIVE guidelines (McGrath et al., 2010). All human embryonic stem cell experimentation was approved by the Biomedical Science Human Ethics Advisory Group, University of Melbourne (approval number 1647041.1).

Materials

Stem cell reagents including Accutase™, BrainPhys™ neuronal medium and Y-27632 were purchased from STEMCELL Technologies (VIC, Australia), Gibco™ natural mouse laminin protein from Life Technologies (VIC, Australia), human fibronectin was from In Vitro Technologies (VIC, Australia), poly-L-ornithine 0.01% solution from Sigma-Aldrich (NSW, Australia) and recombinant human GDF-11 from Lonza (VIC, Australia). Testosterone, 5α-Androstan-17β-ol-3-one (5α-dihydrotestosterone), flutamide, 2-hydroxyflutamide and 4-Nitro-3-(trifluoromethyl) aniline and 17α-Hydroxyprogesterone-d_8 were purchased from Sigma-Aldrich (Australia). Human ARQ24 androgen receptor plasmid (Simeoni et al., 2000) was kindly donated by Professor Angelo Poletti (University of Milan, Italy). Cignal Androgen

Receptor Reporter (luc) Kit was purchased from Qiagen (VIC, Australia) and Dual-Glo® Luciferase Assay System was supplied by Promega Australia (NSW, Australia). Meloxicam animal analgesic was supplied by Troy Laboratories (NSW, Australia). Roche cOmplete™ Mini Protease Inhibitor Cocktail and PhosSTOP™ tablets were purchased from Sigma-Aldrich.

AR luciferase reporter assay in human embryonic stem cell-derived motor neurons

H9 human embryonic stem cells (RRID:CVCL_9773) (Thomson et al., 1998) were differentiated into spinal motor neurons as previously described (Du et al., 2015) with modifications. Briefly, at 5 and 6 days *in vitro* (DIV), culture medium was supplemented with 50 ng/ml GDF11 and SB431543 was removed. Stage 4 (from 19 DIV) medium was changed to BrainPhys® Neuronal Medium (STEMCELL Technologies, Melbourne, Australia). HB9+ and ChAT+ mature motor neurons for this differentiation protocol have been previously quantified and reported by our laboratory (Perera et al., 2017). Here we confirm the expression of specific motor neuron markers ChAT and HB9, as well as AR, as detailed under the relevant experimental sections below.

At 19 DIV (Stage 4, day 1), motor neuron spheres were gently dissociated using accutase digestion and transfected with a 1:1 DNA ratio of human AR construct and luciferase AR reporter construct (assay optimization can be found in supplementary material, Fig S1) using the Neon® Transfection System (Life Technologies, Australia). Briefly, 96-well plates were coated 24 h prior to cell plating with poly-L-ornithine (0.01% w/v), followed by laminin (20 µg/ml) and fibronectin (5 µg/ml) with overnight incubation at 37°C. The cell suspension containing 5 µg DNA/3.75 x 10^6 cells was electroporated using a double 1400 V, 20 ms pulse protocol and plated at 1.5 x 10^5 cells per well in BrainPhys® medium with Y-27632 RHO/ROCK pathway inhibitor. At 24 h post transfection, Y-27632 was removed by full medium

change and cells were treated in duplicate wells with increasing concentrations (variable range from 0.1 nM to 100 µM) of either testosterone, dihydrotestosterone (DHT), flutamide or 2-hydroxyflutamide (HF) alone or flutamide in combination with 10 nM DHT or 50 nM testosterone. Drug stocks were prepared in ethanol with a 0.1% (v/v) final ethanol concentration in treatment medium. At 16 h drug post-treatment, luciferase activity was measured using a Dual-Glo® Luciferase Assay System following the manufacturer's protocol and luminescence detected on a POLARstar Omega Microplate reader (BMG Labtech, Melbourne, Australia). Experiments were repeated in three independent cell differentiations. Firefly luminescence values were normalised against the renilla luciferase construct which acted as an internal control for construct expression and the response relative to untreated controls was determined. To compare AR activation, data were fitted to a log(agonist) vs response curve (Y=Bottom + (Top – Bottom) / [1 + $10^{(Log\ EC50-X)}$]) with bottom constraint set to 1.0 (GraphPad Prism 7, La Jolla, CA). Likewise, to assess effectiveness of AR antagonism, data were fitted to a log(antagonist) vs response curve (Y= Bottom + (Top -Bottom) / [1 + $10^{(X-Log\ IC50)}$]) with top constraint set to 1.0 and bottom constraint > 0.

Immunocytochemistry

Cells at 19 DIV as stated above were plated onto glass coverslips of 1.5 thickness (Marienfield-Superior, Germany) in 48-well plates following coating with poly-L-ornithine, laminin and fibronectin as detailed above. At stage 4, day 3, approximately 48h following plating, cells were fixed for 10 min in 4% paraformaldehyde and washed twice in DPBS. Cells were blocked in 10% normal donkey serum with 0.1% (v/v) Triton-X 100 in 0.1 M PBS and incubated overnight at 4°C in the following primary antibodies; rabbit anti-ChAT (1:500, Millipore Cat# AB143, RRID:AB_2079760), sheep anti-ChAT (1:300, Abcam Cat# ab18736, RRID:AB_2244867), chicken anti-beta III tubulin (1:500, Abcam Cat# ab107216, RRID:AB_10899689), mouse anti-HB9 (5 µg/ml, DSHB Cat# MNR2, RRID:AB_2314625), mouse anti-SMI-

32 (1:1000, BioLegend Cat# 801702, RRID:AB_2715852) and rabbit anti-AR (1:200, Cell Signalling Technology Cat# 5153, RRID:AB_10691711) in antibody diluent 5% (v/v) normal donkey serum with 0.1% (v/v) Triton-X 100 in 0.1 M PBS. Cells were incubated in the following secondary antibodies in the same diluent for 2h at room temperature; anti-rabbit Alexa Fluor®-488 (1:400, Jackson ImmunoResearch Labs Cat# 711-545-152, RRID:AB_2313584), anti-goat DyLight®-550 (1:400, Thermo Fisher Scientific Cat# SA5-10087, RRID:AB_2556667), anti-chicken Cy™3 (1:200, Jackson ImmunoResearch Labs Cat# 703-165-155, RRID:AB_2340363), anti-mouse $F(ab')_2$ fragment Alexa Fluor®-647 (1:400, Jackson ImmunoResearch Labs Cat# 715-606-151, RRID:AB_2340866) followed by 10 min incubation in 1 µg/ml Hoechst 33342 nuclear stain (LifeTech, Cat# H1399). Cells were imaged at 40x magnification on a Leica SP8 confocal microscope.

Animals and drug administration

Transgenic $SOD1^{G93A}$ mice (B6.Cg-Tg(SOD1*G93A)1Gur/J line, stock number 004435, RRID:IMSR_JAX:004435) were purchased from the Jackson Laboratory (Bar Harbor, ME, USA). This model was used for experiments as it remains the only validated mouse model of ALS for preclinical study according to the ALS Therapy Development Institute and recapitulates much of the pathogenesis and pathology of clinical disease. The colony was maintained on a C57BL/6 background at the Florey Institute of Neuroscience and Mental Health Core Animal Services under specific pathogen-free conditions. Experimental animals were group housed in microisolator caging under standard 12 h light-dark conditions with access to food and water *ad libitum*. At postnatal day 60 (P60), male and female $SOD1^{G93A}$ mice were randomised to receive either flutamide or placebo control via surgically implanted subcutaneous slow release drug pellets (100 mg/21 day release; Innovative Research of America, Sarasota, FL, USA). Group sizes were based on the recommended preclinical study guidelines of the ALS Therapy Development Institute (Scott et al., 2008). Briefly, mice were anesthetized under isoflurane and

drug pellets were inserted laterally under the skin of the upper back via an incision at the back of the neck. A single-dose of meloxicam (3 mg/kg, s.c. above the hindlimb) was given prior to incision to manage post-operative pain. Pellets were surgically replaced every 21 days until mice reached clinical endpoint or a specified tissue collection timepoint. Serial blood collection (50-200 µl) was performed by submandibular bleed prior to drug administration and every 28 days until clinical endpoint. This part of the study was performed unblinded due to the distinctive yellow colour of flutamide and excreted metabolites, compared to the drug-void placebo pellet. Animals were killed by administering a lethal dose of sodium pentobarbitone (100 mg/kg, i.p.) and either i) organs collected, weighed and snap frozen in dry ice, ii) animal was transcardially perfused with 0.1 M PBS and tissue collected and snap frozen for LC-MS-MS analysis or iii) animal was transcardially perfused with 0.1 M PBS followed by 4% paraformaldehyde in 0.1 M PB with 1-2 h post-fix and cryoprotected in a sucrose gradient 10%, 20% and 30% in PBS for up to 5 days prior to snap freezing in isopentane cooled in dry ice.

Behavioural and survival analyses

Mice were assessed weekly from treatment initiation for body weight change and motor performance. Motor co-ordination and function were determined on a Rota-Rod 47600 (Ugo Basile, Italy) with training as previously described (Perera et al., 2017). Mice were placed on an accelerating rod (4-40 rpm) over a 5 min period. An average of 2 trials was conducted over a 1 h period and latency to fall was recorded for each animal. The appearance of disease onset was retrospectively determined using the age of maximal body weight which is a reliable and objective measure of muscle denervation onset, as previously described (Turner et al., 2014). Clinical endpoint criteria for survival analysis in $SOD1^{G93A}$ mice were defined as the onset of paralysis in hindlimbs and/or the cumulative loss of 20% peak body weight. One female mouse from the flutamide treatment group was found dead without previous signs of clinical endstage and was excluded from survival analysis.

Testosterone, flutamide and metabolite assessment in plasma

At blood collection, EDTA (2.5 µmol/tube) was used as an anticoagulant and plasma was isolated by centrifugation at 1150 x *g* for 10 min following collection and stored at -80°C. For extraction of total testosterone and flutamide, plasma aliquots of 25 µl were vortexed for 1 min in 200 µl of Methyl-Tert-Butyl Ether (MTBE) containing 100 pg/ml of 17α-Hydroxyprogesterone-d_8 used as an internal standard. Following 10 min centrifugation at 21,000 x *g* the supernatant was collected, and the process was repeated on the remaining aqueous fraction. Combined supernatants were dried down using a rotary evaporator under 200 mbar, and pellets reconstituted in 100 µl of 50/50 (v/v) acetonitrile and water.

Testosterone, flutamide and flutamide metabolites (Tevell et al., 2006) were analysed by Ultra High Pressure-Liquid Chromatography (UHPLC) MS-MS. UHPLC-MS-MS coupled with an Agilent 6490 triple quadrupole (QQQ) mass spectrometer. Liquid chromatography was performed on an Agilent UHPLC system equipped with a 1290 Infinity II pump, degasser, an autosampler and a temperature-controlled column compartment. Chromatographic separation for testosterone, flutamide and flutamide metabolites was achieved on an Agilent Poroshell 120 C18 (2.1 µ, 1.8 id x 100 mm) column connected with a guard column. The column oven temperature was maintained at 35°C and the injection volume was set to 10 µl. A gradient mobile phase consisting of 1 mM ammonium fluoride in water (A) and methanol (B), at a flow rate of 0.25 ml/min was used.

Quantitation of the target analytes was performed in multiple reaction monitoring (MRM) mode on an Agilent Jet Stream/ESI source in dual (positive and negative) mode. The specific MRM transitions for testosterone, flutamide, 2-hydroxyflutamide, 4-nitro-3-(trifluoromethyl)-aniline (Flu-1) and 17α-Hydroxyprogesterone-d_8 (internal standard) were monitored (20 ms dwell time/transition) at *m*/*z* 289.1 >108.8, 275 > 204.8, 291 > 204.8, 205 > 204.8 and 339 > 100.1, respectively. All analyses were quantified

using retention times and the ratios of selected precursor and product ions with those of standards. Data analysis was performed using Agilent Mass Hunter software (version B. 07.1, RRID:SCR_015040). Total testosterone in plasma was calculated based on solvent standards adjusted for extraction and processing recovery from plasma spiked standards, with a limit of quantitation at 27 pg/ml (details provided in supplementary material). Flutamide and metabolites, HF and Flu-1 concentrations were determined based on a blank plasma spiked standard curve (Tables S2-S4).

Testosterone, flutamide and metabolite assessment in spinal cord

In animals treated for 2 weeks with either placebo or flutamide, ~30 mg of frozen spinal cord tissue was homogenised in 500 µl of ice cold MTBE containing 100 pg/ml of internal standard. Samples were placed in Lysing Matrix D, 2 ml tubes (MP Biomedicals, Australia) and homogenised in a Precellys® 24 homogeniser with cryolysis cooling (Bertin Technologies, France) using the 6800 rpm, 3 x 30 sec programme at -10 °C. Homogenates were centrifuged at 21,000 x *g* for 10 min and supernatant was removed and pellet fraction was vortexed for 1 min in a second 500 µl internal standard containing aliquot of MTBE and centrifuged. Pooled supernatants were dried down and resuspended in 100 µl of 50/50 (v/v) acetonitrile and water before analysis by UHPLC-MS-MS as described above. Total testosterone, flutamide, HF and Flu-1 concentrations were determined in tissue based on solvent and blank tissue spiked standards and presented as ng/g tissue amounts.

Protein extraction and immunoblot analysis

Cells were lysed in Triton-X lysis buffer (20 mM Tris-Cl, 150 mM NaCl and 1% Triton-X 100) containing protease and phosphatase inhibitor cocktail tablets (Roche) for 20 min on ice. Supernatants obtained following centrifugation (21,000 x *g* for 20 min at 4°C) were quantified for protein using the Direct Detect® Infrared Spectrometer (Millipore). For tissue, gastrocnemius muscle was firstly pulverised

mechanically in liquid nitrogen prior to processing for biochemical assays. Spinal cord and muscle tissue were homogenized by sonication in ice-cold RIPA buffer (50 mM Tris-Cl, pH 7.4, 150 mM NaCl, 0.1% SDS, 1% sodium deoxycholate and 1% Triton-X 100) with the addition of protease and phosphatase inhibitor cocktail tablets. Sonication was conducted at 50% amplitude (Q55 Sonicator, Sonica, Newtown, CT, US) with brief pulses applied over 10-15 sec until tissue particulates were no longer visible and samples incubated on ice for 20 min before centrifugation at 21,000 x *g* for 20 min at 4□C. Supernatants from tissue were collected and quantified for total protein using the BCA assay according to the manufacturer's protocol (Pierce® BCA assay kit, Thermo Fisher, Cat# 23225). Protein lysates were denatured by boiling in Laemmli buffer containing 2% (v/v) β-mercaptoethanol and 50 µg protein was electrophoresed through 4–20% Mini-PROTEAN® TGX Stain-Free™ gels for cell lysate or 4–15% Criterion™ TGX Stain-Free™ gels for tissue lysate (Bio-Rad Laboratories, NSW, Australia) and transferred onto PVDF membrane at 25 V for 16 min using a Trans-Blot® Turbo™ Transfer System (Bio-Rad). Total protein transferred onto membrane was imaged on a ChemiDoc™ MP Imaging System (Bio-Rad Laboratories, NSW, Australia) prior to blocking with 5% low-fat milk powder in TBST for 1 h at room temperature and probed with rabbit primary antibody against AR (1:1000 unpurified, Abcam, cat# ab133273, RRID:AB_11156085), or antibody against human-AR (1:1000) and anti-HB9 antibody (1:50), both detailed above, using a SignalBoost™Immunoreaction Enhancer Kit (Merck Millipore, Cat# 407207) overnight at 4□C. Mouse androgen receptor detection by immunoblotting was validated using testis tissue and AR knockout tissue as a positive and negative control, respectively. Membranes were probed with StarBright™ Blue 700 goat anti-rabbit secondary antibody (1:5000, Bio-Rad, Cat# 12004161, RRID:AB_2721073) and DyLight 800 goat anti-mouse secondary antibody (1:5000, Bio-Rad, Cat# STAR117D800GA, RRID:AB_10845157) for 1 h at room temperature and imaged on a ChemiDoc™ MP. Primary antibody diluents were used sequentially up to three times for immunoblotting. For analysis, background adjusted total AR band intensity was normalised against background adjusted total lane

protein intensity using Image Lab 6.0 software (Bio-Rad, www.bio-rad.com/en-au/product/image-lab-software, RRID:SCR_014210). Average group values were then expressed fold relative to averaged control group values (expressed as 1.0) to interpret any changes in protein abundance occurring in flutamide treated animals.

RNA extraction and qPCR analysis

RNA was extracted from cell cultures using the RNeasy Mini Kit (Qiagen, Cat# 74104) and from 30 mg gastrocnemius muscle using RNeasy Fibrous Tissue Mini Kit (Qiagen, Cat# 74704) according to manufacturer's protocol with homogenisation of tissue using the TissueLyserLT (Qiagen) for 5 min at 50 Hz. cDNA was reverse transcribed using iScript™ Reverse Transcription Supermix (Bio-Rad, Cat# 1708841) under the following PCR conditions; 5 min at 25°C, 30 min at 42°C and 5 min at 85°C. qPCR was performed using SsoAdvanced™ Universal SYBR® Green Supermix (Bio-Rad, Cat# 1725270) and 20 µl reaction volume containing 400 nM of each primer was run using CFX Manager™ 3.1 software (RRID:SCR_003375) provided with a CFX96™ Touch Real-Time PCR Detection System (Bio-Rad). Primers were designed using Primer3 v0.4.0 design tool (http://bioinfo.ut.ee/primer3-0.4.0/, RRID:SCR_003139) to cover majority of RefSeq transcript variants (UCSC Genome Browser, http://genome.ucsc.edu/, RRID:SCR_005780) as described in Table 1. Samples were run in triplicate and data were expressed in Ct values normalised to *Gapdh* or *Hprt1* housekeeping gene for cells and tissue, respectively, and fold change between control and treated groups determined using the $2^{-\Delta\Delta Ct}$ method. Validation of *Gapdh* as the most viable housekeeping gene for comparisons across undifferentiated embryonic stem cell to mature motor neurons can be found in Supplementary material (Table S1).

Spinal cord immunohistochemistry and image quantification

Lumbar spinal cord tissue was cryosectioned at 20 µm with 1:10 series mounted onto poly-L-lysine coated slides. For AR staining, antigen retrieval was performed by baking slides for 2 h at 95 °C in citrate buffer (10 mM citric acid, pH 6.0). Sections were blocked in 6% (v/v) normal donkey serum in 0.3% (v/v) Triton-X 100 in 0.1 M PBS for 1 h room temperature. An additional endogenous avidin-biotin blocking step (Endogenous Avidin/Biotin Blocking Kit, Abcam, Cat# ab64212) was performed according to manufacturer's protocol. Primary antibodies including; rabbit anti-AR (1:100 unpurified, Abcam, Cat# ab133273), goat anti-ChAT (1:100, Millipore, Cat# AB144P, RRID:AB_2079751), rat anti-GFAP (1:500, Zymed, Cat# 13-0300) and rat anti-CD11b (1:100, Bio-Rad, Cat# MCA711, RRID:AB_321292) were prepared in 2% (v/v) normal donkey serum in 0.3% (v/v) Triton-X 100 in 0.1 M PBS for a single use 48 h incubation at 4 °C. An additional 3 h incubation at room temperature with donkey biotinylated-anti-rabbit (1:100, Jackson ImmunoResearch Cat# 711-065-152, RRID:AB_2340593) was included to amplify the AR detection. Secondary antibodies were incubated for 2 h at room temperature in the same antibody diluent, including; streptavidin Alexa Fluor®-488 (1:200, Jackson ImmunoResearch Cat# 016-540-084, RRID:AB_2337249), anti-goat DyLight®-550 (1:200), and anti-rat Alexa Fluor®-647 (1:200, Jackson ImmunoResearch, Cat# 712-605-153, RRID:AB_2340694). For AR quantification, AR staining detectable in the nucleus of ChAT-expressing motor neurons was counted through L1-6 spinal cord ventral horns (~40 sections per mouse). Quantification of ChAT-positive motor neurons was determined by counting and averaging 10 sections (equivalent to 10 ventral horn pairs) selected at equally spaced intervals spanning L1-6 under 20x magnification. GFAP-positive astrocyte and CD11b-positive microglia images were acquired at 40x magnification with Z-stacked fields taken at 0.54 µm per step through an 8 µm stack (i.e. 15 images stacked together). An average of 10 fields were counted from separate ventral horns selected at equally spaced intervals spanning L1-6 and expressed as cells per mm^2 area. All images were captured by the Zeiss AxioObserver Z1 (Carl Zeiss Pty Ltd, North Ryde, Australia).

Muscle immunohistochemistry and image quantification

Unperfused gastrocnemius muscle was collected and embedded in OCT prior to snap freezing in isopentane cooled over dry ice. Cross-sections of 12 µm, 1 in 12 series, were slide mounted and dried for 1 h at room temperature and either stored at -80 °C or processed for immunostaining. Slides were drop fixed in neutral-buffered formalin for 10 min and rinsed in PBS. Sections were processed as described in previous setting without antigen-retrieval step for AR staining. For AR staining quantification, sections were co-incubated in anti-AR (as above) and rat anti-laminin (1:200, Abcam, Cat# ab11576, RRID:AB_298180) for 48 h at 4 °C. Secondary antibody incubation was as described above, followed by 15 min incubation in 1 µg/ml Hoechst 33342 nuclear stain. A series of 5 randomly selected images were taken at from a single muscle cross-section per animal, with treatment group blinding, at 40x magnification on a Zeiss AxioObserver Z1 and total nuclei were determined by semi-automated particle analysis using ImageJ software (RRID:SCR_003070) followed by manual counting of AR positive nuclei. For analysis of fibre cross-sectional area, sections were immunolabelled with rabbit anti-laminin (1:500, Abcam, Cat# ab11575, RRID:AB_298179) to delineate the basement membrane, followed by anti-rabbit secondary as detailed above. Semi-automated analysis was performed using ImageJ software following the methodology described previously by Tyagi and colleagues (Tyagi et al., 2017), including a slight modification to the macro to allow fibres within the range of 100-20,000 μm^2 to be captured. A total of 5 randomly selected fields of view were taken at 20x magnification and averaged as representation of the gastrocnemius cross-section, allowing ~800-1,000 fibres to be quantified per animal. Neuromuscular junction (NMJ) staining was performed on 4% PFA perfused tissue with 24-48 h cryoprotection in 20% sucrose in 0.1 M PB before rapid freezing in OCT. Fibres were longitudinally cryosectioned at 50 µm, 1 in 6 series and slide mounted prior to staining. Sections were permeabilised in 2% Triton-X 100 in PBS for 30 min, followed by blocking in 5% normal donkey serum/3% BSA with 1%

Triton-X 100 in PBS for 1 h at room temperature. Primary antibody incubation with anti-neurofilament heavy chain (1:500, Abcam, Cat# ab8135, RRID:AB_306298) and anti-synaptophysin (1:200, Abcam, Cat# ab32594, RRID:AB_778204) was conducted overnight at 4□C in diluent containing 2% donkey serum/3% BSA/1% Triton-X 100 in PBS. Triplicate 15 min wash steps were followed by a 2 h incubation in anti-rabbit DyLight®-550 secondary antibody (1:200, Thermo Fisher Scientific Cat# SA5-10039, RRID:AB_2556619) and 488-conjugated α-bungarotoxin (1:1000, LifeTech, Cat# B13422). Images were acquired at 20x magnification on a Leica SP8 confocal microscope with Z-stacked fields taken at 2 µm per step through 20 µm stack (i.e. 10 images stacked together). An average of 10 fields were imaged per animal allowing approximately 100 NMJs to be analysed as fully innervated, partially innervated or denervated.

Data and statistical analyses

The data and statistical analysis comply with the recommendations on experimental design and analysis in pharmacology (Curtis et al., 2015). All analyses were performed using GraphPad Prism 7.0 software (San Diego, CA, USA, RRID:SCR_002798) and data presented as mean ± SEM. Survival of flutamide and control treated mice was compared using log-rank (Mantel Cox) test with median values reported. Western blot data, ages to peak body weight and rotarod activity, motor neuron and glial cell counts were analysed using two-way ANOVA with Fisher's least significant difference (LSD) test for planned comparisons between control and flutamide or male and female where *F*-value indicated a significant difference ($P<0.05$). Tissue weight, plasma testosterone concentrations over time and myofibre diameter frequency in males was analysed by two-way ANOVA with Fisher's LSD test comparing control with flutamide group at each time interval or fibre diameter, respectively, where *F*-value indicated a significant treatment difference. All other comparisons between control and flutamide treated means were using two-tailed Student *t*-test. In cases where a parametric test could not be used as significantly

different variances occurred between groups, a Mann Whitney test was used to compare control and flutamide group means. Only statistically significant data are reported for means including n=5 with $P<0.05$ taken as statistical significance.

Nomenclature of Targets and Ligands

Key protein targets and ligands in this article are hyperlinked to corresponding entries in http://www.guidetopharmacology.org, the common portal for data from the IUPHAR/BPS Guide to PHARMACOLOGY (Harding et al., 2018), and are permanently archived in the Concise Guide to PHARMACOLOGY 2017/18 (Alexander et al., 2017).

RESULTS

Implantable flutamide pellets result in steady state flutamide and hydroxyflutamide plasma levels and pharmacologically active concentrations in the spinal cord

We first established effective concentrations of flutamide to block androgen-induced AR activation *in vitro* to extrapolate to spinal cord *in vivo*. Human embryonic stem cell (hESC)-derived motor neurons were validated for expression of motor neuron specific markers both at transcript and protein level (Fig 1A-E) including ChAT and HB9. This data was in line with previous quantification of this differentiation protocol by our laboratory where we reported 80% and 69% neurons positive for ChAT and HB9, respectively (Perera et al., 2017). hESC-derived motor neurons also expressed endogenous AR which was elevated by DHT treatment (Fig. 1D) and was predominantly nuclear as expected (Fig. 1F). hESC-derived motor neurons expressing an AR-activated luciferase reporter showed concentration-dependent responses to the AR agonists, testosterone and DHT (Fig 1G). DHT showed a 10-fold greater potency, compared to testosterone, with maximal activation occurring from 10-100 nM, respectively. This reflects previous AR binding and potency data (Gao et al., 2005). The flutamide metabolite, HF, showed weak agonist activity at high concentrations 10-100 µM in the absence of AR agonist, as previously described (Culig et al., 1999) (Fig 1G). Flutamide revealed poor antagonist activity and was only effective at a single high dose concentration of 100 µM with HF showing dose-dependent inhibition of

AR activation with a 50-100-fold higher antagonist potency, compared to flutamide (Fig 1H,I). Based on the IC_{50} (provided in Fig 1) an 11-fold and 36-fold molar excess of HF would be required to block 50% AR activation by 50 nM testosterone (Fig 1H) or 10 nM DHT (Fig 1I), respectively. For full AR inhibition, approximately 200-fold and 1000-fold molar excess of HF would be anticipated to inhibit testosterone and DHT, respectively, based on maximal inhibitory responses achieved at 10 µM HF in hESC-derived motor neurons.

Next, male $SOD1^{G93A}$ mice were implanted with slow release placebo control or flutamide pellets from postnatal day 60 (P60) using a dose regimen (5 $mg.d^{-1}$, s.c.) effective in mouse models of SBMA (Reiner et al 2014). Importantly, this dose of flutamide does not affect body weight and motor function in wild-type mice (Reiner et al 2014). Plasma levels of testosterone, flutamide and its metabolites were first serially measured in implanted mice. Antagonism of AR in the hypothalamic gonadotropin-releasing hormone neurons results in disinhibition of androgen production via the HPG axis and systemic testosterone release by the testes (Supplementary material Fig S2). We confirmed a significant early elevation in circulating testosterone levels in response to flutamide treatment with a 6-fold increase, compared to control mice observed at P74, or 2 weeks post-treatment initiation (Fig 2A). A 2.5-fold elevation in testosterone levels persisted in flutamide treated mice at P88, or 4 weeks post-treatment initiation. Circulating testosterone levels were comparable in flutamide and control male mice from P116 onwards. Over the course of the study, flutamide was maintained at a steady state plasma concentration of approximately 100 $ng.ml^{-1}$, with metabolites HF at approximately 50-fold higher level and pharmacologically inactive, Flu-1, maintained at 10-fold lower plasma concentration, relative to flutamide (Fig 2B). The levels of testosterone and drug in spinal cord tissue at 2 weeks post-treatment reflected systemic circulating levels (Fig 2C). Importantly, there was a ~250-fold molar excess of HF in

spinal cord relative to testosterone, consistent with effective displacement of testosterone for AR binding and activation based on the hESC-derived motor neuron AR activation assay.

Flutamide decreases prostate and seminal vesicle weights in male SOD1^{G93A} mice

The prostate and seminal vesicles (SV) are highly responsive to circulating androgens with weights reflecting circulating testosterone levels (van Roijen et al., 1997). Given that flutamide treatment elevates circulating testosterone levels, SV weight in the current study reflected the systemic effects of flutamide antagonism of AR. SV weight showed a significant 30% reduction following 2-weeks of flutamide treatment (P74) and a 50% reduction at 2-months post-treatment (P120; Fig 3A,B). Systemic AR antagonism was also reflected in flutamide-treated male prostate weights, with a significant 30-40% reduction, compared to control males at P74 and P120 (Fig 3C). While the testis is responsible for testosterone production and regulation from the HPG feedback system, we confirmed no change in testis weight over the duration of treatment (Fig 3D), in line with previous studies (Marchetti & Labrie, 1988).

Flutamide reduces AR levels in skeletal muscle and spinal cord of male SOD1^{G93A} mice

We next determined AR expression levels in skeletal muscle and spinal cord in response to flutamide treatment in SOD1^{G93A} mice. AR was detected in both male and female gastrocnemius muscles and spinal cord as a single ~110 kDa monomer (Fig 4A). As expected, AR levels were consistently and significantly ~50% lower in females, than males, in both skeletal muscle and spinal cord. Gastrocnemius muscle AR protein levels were similar in gastrocnemius muscles, irrespective of treatment at P74 (Fig 4A,B). AR protein levels were reduced in male mice treated with flutamide at P120, although not statistically significant (Fig 4C,D). In spinal cord, AR levels were significantly decreased by 23% in male flutamide treated mice, compared to control male mice at P74 (Fig 4E,F). In contrast, AR expression in

503 female spinal cord was not affected by flutamide treatment at P74. Lastly, AR protein accumulation was
504 again similarly decreased, although not statistically significantly, in spinal cords of flutamide treated
505 male animals, compared to untreated male mice at P120 (Fig 4G,H).
506
507 To determine whether AR nuclear translocation was affected by flutamide in skeletal muscle and spinal
508 cord, we examined the subcellular distribution of AR in male SOD1^{G93A} mice at P120 (Fig 4I-M). In
509 concert with immunoblotting results in gastrocnemius muscle, there was a significant 50% reduction in
510 the number of AR+ myonuclei in flutamide-treated males, compared to controls (Fig 4J), which was
511 independent of the total number of nuclei present in the muscle (Fig 4K). Flutamide treatment did not
512 significantly affect the percentage of AR+ nuclei in ChAT+ motor neurons in the spinal cord (Fig 4L) with
513 approximately 15% of total motor neurons showing AR-immunoreactive nuclei in both flutamide and
514 control treated mice (Fig 4M); total ChAT+ motor neuron counts are reported in Fig 9A. AR
515 immunoreactivity was largely undetectable in gastrocnemius myocytes and spinal cord motor neurons
516 of female mice (data not shown).
517
518 **Flutamide treatment accelerates disease onset and motor dysfunction in male SOD1^{G93A} mice**
519 The effect of flutamide treatment on disease onset, progression and survival was next assessed in
520 SOD1^{G93A} mice. The mean disease onset, determined by the age of weight loss onset, was significantly
521 hastened by 19 days in flutamide treated male mice, compared to control males (Fig 5A). Flutamide did
522 not affect disease initiation in female mice, compared to control females. Flutamide did not show a
523 significant reduction in the absolute body weights of male and female mice compared to their control
524 counterparts, although male mice showed a significant interaction effect between treatment and time
525 by two-way ANOVA (P=0.0321; Fig S3A and B). A comparison of locomotor function at disease onset in
526 flutamide treated males revealed a significant treatment interaction effect with a deficit in rotarod test

performance, compared to control males (Fig 5B). There was no impact of flutamide on locomotor function of female mice at disease onset. Neither male, nor female, mice showed a significant treatment interaction with declining locomotor function over the duration of the disease (Fig S3 C and D).

Kaplan-Meier analysis of disease onset showed an earlier median onset of disease in flutamide (84 days) compared to control male mice (112 days) (P=0.06 determined by the Log-rank (Mantel-Cox) test) (Fig 5C). Median survival, determined by the time to reach hindlimb paralysis onset, was comparable in flutamide (159 days) and control male mice (155 days; Fig 5E). Kaplan-Meier analysis of median disease onset in females revealed no difference in flutamide (116 days) and control mice (119 days) (Fig 5 D). The median lifespans of flutamide (161 days) and control female mice (160.5 days) were also similar (Fig 5F). Thus, flutamide affects disease onset, but not outcome, specifically in male $SOD1^{G93A}$ mice.

Flutamide exacerbates hindlimb muscle atrophy in male $SOD1^{G93A}$ mice

To address how flutamide accelerates disease onset and motor deficits in male $SOD1^{G93A}$ mice, we examined skeletal muscle for atrophy markers. In $SOD1^{G93A}$ mice, the upregulation of transcripts for TGFβ1, myogenin (MYOG) and myoblast determination protein 1 (MyoD) in skeletal muscle reflects atrophy (Galbiati et al., 2012). In the gastrocnemius muscle of male mice at P120, flutamide caused a significant ~1.5-fold upregulation of atrophy markers TGFβ1 (Fig 6A), MYOG (Fig 6B) and MyoD (Fig 6C), compared to controls. In contrast, there was no significant change in expression of atrophy markers in gastrocnemius muscle of female $SOD1^{G93A}$ mice with flutamide treatment, with exception of MyoD which was downregulated by ~0.3-fold (Fig 6D-F). To correlate upregulation of these muscle atrophy markers with muscle pathology in male mice, we analysed myofibre cross-sectional properties in gastrocnemius muscles at P120 (Fig 6G). Fibre number per area unit quantified was significantly increased by 20% per in flutamide treated male mice, relative to control males (Fig 6H). Importantly,

there was a significant 24% reduction in the mean fibre cross-sectional area (CSA) in flutamide treated males, compared to controls (Fig 6I). The minimum ferret diameter, which minimises the potential impact of oblique tissue sectioning, was also significantly lower by 12% in flutamide treated males, compared to controls (Fig 6J). A stratification of muscle fibre diameters showed flutamide treated males had a significantly greater frequency of fibres with a CSA ≤1000 μm^2 and less fibres ≥4000 μm^2 (Fig 6K). These findings collectively suggest that flutamide may exacerbates the clinical phenotype of male $SOD1^{G93A}$ mice by promoting disease progression and/or skeletal muscle wasting.

Effects of flutamide on denervation and motor neuron survival in male $SOD1^{G93A}$ mice

The impact of flutamide on neuropathology was next examined in male $SOD1^{G93A}$ mice. Denervation of muscle fibres by motor neuron terminals alters the expression of several genes within the muscle tissue. A switch in nicotinic acetylcholine receptor (nAChR) from alpha to gamma subunits, elevation in neural cell adhesion molecule (NCAM1) and muscle specific kinase (MuSK) are key markers of denervation (Aare et al., 2016). In flutamide treated male mice, there was no significant difference in nAChRγ or MuSK transcript levels in gastrocnemius muscle, although a significant 1.3-fold increase in NCAM1 levels occurred, compared to control males (Fig 7A-C). Morphological innervation was also examined in longitudinal sections of gastrocnemius muscles collected from male mice. Innervation was determined by the colocalisation of the muscle motor endplate labelled with α-bungarotoxin (BTX) and the motor neuron synaptic terminals labelled with synaptophysin (Fig 7D). There was a trend toward increased denervation in muscles of flutamide treated males, compared to control males, although this was not significant (Fig 7E).

Effects of flutamide on motor neuron survival and glial cell activation in male $SOD1^{G93A}$ mice

The effects of flutamide on spinal cord pathology were next evaluated in male SOD1^{G93A} mice. ChAT-positive motor neurons were counted across spinal cord region L1-L6. No significant treatment related changes were observed, although a sex-specific difference revealed that motor neuron counts were significantly higher in flutamide treated males, compared to flutamide treated female mice (Fig 8A,B). Astrocyte activation assessed by GFAP immunohistochemistry in spinal cord was similar in flutamide and control mice, however, GFAP-positive cell counts were lower in control female mice, compared to control males (Fig 8C,D). Microgliosis shown by CD11b immunohistochemistry was also similar in flutamide and control mice, irrespective of sex (Fig 8E,F). Thus, flutamide treatment promotes skeletal muscle pathology, but not central pathology, in this mouse model of ALS.

DISCUSSION

There is clear epidemiological, genetic and biological evidence for a key role of androgens and AR signalling in ALS. Firstly, ALS is more common in males with an earlier age of onset in both male patients and mouse models, implicating androgen influences in disease (McCombe & Henderson, 2010). Secondly, mutations in AR cause lower motor neuron loss in SBMA which shows some pathological overlap with ALS, suggesting defects in AR can trigger motor neuron degeneration (Beitel et al., 2013; Cortes & La Spada, 2014). Lastly, administration of androgens to SOD1^{G93A} mice ameliorates disease progression (Yoo & Ko, 2012). Our study is the first to date to assess the impact of anti-androgen treatment on a mouse model of ALS to clarify the contribution of AR signalling. Chronic administration of the AR antagonist, flutamide, to presymptomatic SOD1^{G93A} mice accelerated disease onset and motor dysfunction in male mice, with a concomitant exacerbation of hindlimb skeletal muscle pathology. Interestingly, flutamide worsened peripheral, but not central, pathology in male SOD1^{G93A} mice, reflecting the contribution of skeletal muscle pathology to disease onset and outcome in this mouse model of ALS.

598

599 We employed a dose of flutamide which was effective in three different mouse models of SBMA (Renier
600 et al., 2014). Importantly, this flutamide dose does not affect body weights or locomotor function in
601 wild-type (WT) mice (Renier et al., 2014), allowing us to distinguish mutant SOD1-specific effects from
602 impacts on general physiology. This sustained-release pellet preparation was estimated to release ~4.7
603 mg of drug per day over 21 days, thereby exposing mice to a dose of ~180-230 $mg.kg^{-1}$ based on weight
604 distributions. Limited studies have determined the pharmacokinetics of flutamide in mice, which is
605 critical in providing effective drug antagonism of AR to compete with local androgens for receptor
606 binding. A single oral dose of 20 $mg.kg^{-1}$ flutamide administered to mice yielded a peak plasma
607 concentration below 0.5 $\mu g.ml^{-1}$ for flutamide and 4.5 $\mu g.ml^{-1}$ for HF (Matsuzaki et al., 2006). Based on
608 this, Renier and colleagues estimated that the sustained release flutamide formulation would generate
609 serum levels of approximately 30 $\mu g.ml^{-1}$ (Renier et al., 2014) which is 300-fold higher than the 0.1
610 $\mu g.ml^{-1}$ measured plasma steady state concentrations in this current study. As flutamide has a short
611 half-life *in vivo* due to its rapid metabolism to HF in the liver, in addition to undergoing first pass-
612 metabolism following oral administration (Schulz et al., 1988), making predictions based on single oral
613 doses limited. Indeed, the steady state plasma levels of HF were approximately 50 times higher than
614 parent compound in the current study. This is similar to the human pharmacokinetics that show
615 consistently higher levels of both metabolites, HF and Flu-1, compared to parent compound (Aizawa et
616 al., 2003; Asade et al., 1991), and in rats where HF reaches 70-fold higher tissue concentrations
617 compared to flutamide (Neri, 1989). In contrast to human data, the metabolite Flu-1, was lower than
618 that of flutamide and may reflect differences between human and rodent metabolism.

619

620 Evidence of systemic antagonism of AR was reflected by significantly reduced prostate and seminal
621 vesicle weights of flutamide treated male $SOD1^{G93A}$ mice. The relationship between the mechanism of

action of flutamide and its effect on both AR protein stability and nuclear translocation have been a subject of debate. In a SBMA mouse model receiving 1.8 mg of flutamide every second day, SV and prostate showed reduced weights, with no effect on AR levels in spinal cord or muscle (Katsuno et al., 2003). Flutamide administered at efficacious levels by a continuous slow-release formulation, showed reductions in both soluble AR levels in spinal cord and muscle and decreased mutant AR aggregates only in muscle (Renier et al., 2014). In the current study, plasma and spinal cord levels of testosterone following 2-weeks of flutamide administration were elevated, compared to control mice, similar to those observed in SBMA models (Renier et al., 2014). Likewise, we confirmed a decrease in the levels of soluble AR in the spinal cord of these mice, indicative of flutamide-induced reduction in AR protein stability.

In muscle tissue, AR expression occurs in some mature myofibres, but more extensively in the mesenchymal precursor satellite cells (Sinha-Hikim et al., 2004), whereby androgens promote myogenesis and differentiation into mature skeletal muscle tissue. In ALS, skeletal muscle undergoes both intrinsic metabolic disturbances, as well as degeneration in response to denervation. Denervation of the gastrocnemius muscle is reportedly detectable as early as P50 in $SOD1^{G93A}$ mice (Frey et al., 2000) before obvious symptoms manifest. In response, myogenesis occurs to replace the lost myofibres (Pun et al., 2006) and the satellite cell marker, PAX7, is upregulated in presymptomatic $SOD1^{G93A}$ mice (Manzano et al., 2011). Satellite cells also showed an intrinsic loss in proliferative capacity in $SOD1^{G93A}$ mice (Manzano et al., 2013). Hence, there is strong evidence for a potential role for AR in early ALS pathogenesis. This was confirmed in the current study, as we show that flutamide can accelerate disease onset and motor deficits in male mice, with concomitant exacerbation in myofiber atrophy. Castration in $SOD1^{G93A}$ mice has shown to both induce muscle hypotrophy (Yoo & Ko, 2012) and have no effect on clinical parameters (Aggarwal et al., 2014) and may reflect influences from genetic background

of mice on the transgene (Pfohl et al., 2015). To date, castration has consistently failed to modify disease onset or survival in male SOD1^{G93A} mice (Aggarwal et al., 2014; Sheean et al., 2015; Yoo & Ko, 2012). The reasons for the lack of effect seen in these studies compared to our study showing exacerbated disease onset may be complex. For instance, castration may disrupt the source and production of other steroid hormones such as estrogens which is produced from testosterone metabolism, as well as the testis being a source of androstenedione and progesterone (Murphy & O'Shaughnessy, 1991). Their influences on disease progression cannot be discounted. In gonadally intact mice androgens may also signal via alternative pathways, for example, the membrane-located androgen receptors (mAR) which function as G-protein coupled receptors, rather than AR, a nuclear receptor, activating the classical genomic pathway (Pi & Quarles, 2012; Wang et al., 2014).

Many experimental therapies tested over the past decade, which have specifically targeted muscle pathology in ALS have been unsuccessful in modifying survival in ALS rodent models. Muscle targeted expression of the transcriptional coactivator, peroxisome proliferator-activated receptor gamma coactivator-1α (PGC-1α), in SOD1^{G37R} mice improved mitochondrial biogenesis, muscle atrophy and function , but did not impact upon disease onset, muscle innervation, motor neuron or glial cell pathology (Da Cruz et al., 2012). Skeletal muscle or CNS restricted IGF-1 overexpression did not change disease onset or motor neuron survival in SOD1^{G93A} mice (Messi et al., 2007), in contrast to an earlier study which showed positive effects of muscle-specific IGF-1 expression on survival (Dobrowolny et al., 2005). Blocking the effect of myostatin, a muscle growth inhibitor, increased muscle mass and strength in both SOD1^{G93A} mice and rats, with no change in disease onset or survival (Holzbaur et al., 2006). A robust delay in disease onset occurred in SOD1^{G93A} mice overexpressing the antioxidant regulating transcription factor, nuclear factor erythroid 2-related factor 2 (Nrf2), specifically in vulnerable fast type II myofibres, however, no change in survival was observed (Vargas et al., 2013). Taken together, these

studies demonstrate that while muscle targeted therapies may have a modulatory influence on disease progression and in many cases muscle atrophy, they are most often unable to halt motor neuron loss, the underlying cause of hindlimb paralysis or clinical endstage in these mice. Alternatively muscle-derived therapies or delivery strategies which specifically target preservation of NMJ structure and motor axons, present more promising approaches to extend survival in $SOD1^{G93A}$ mice, as supported by benefits of MuSK stimulation, a receptor kinase important in NMJ maintenance (Cantor et al., 2018) and muscle delivery of retrogradely transported neurotrophic growth factors (Acsadi et al., 2002; Azzouz et al., 2004; Kaspar et al., 2003; Pun et al., 2006).

The recent evidence that myopathic features in SBMA strongly play a role in driving disease processes (Cortes et al., 2014) has once again raised question to the potential role of skeletal muscle in non-cell autonomous mechanisms in other motor neuron degenerative disorders, including ALS (Cortes & La Spada, 2014). Similarly to muscle-restricted expression of polyQ-expanded AR causing disease phenotype in SBMA, muscle-restricted overexpression of $SOD1^{G93A}$ was able to induce muscle atrophy and dysfunction through oxidative stress (Dobrowolny et al., 2008), identifying muscle as a primary target in ALS. However, other studies which used several approaches to specifically target $SOD1^{G93A}$ transgene in the skeletal muscle showed no therapeutic survival benefits (Miller et al., 2006; Towne et al., 2008). A more recent study by Dobrowolny and colleagues showed that muscle-specific $SOD1^{G93A}$ transgene expression was able to modulate transcript expression in the spinal cords of mice (Dobrowolny et al., 2015) supporting the notion that muscle signalling is able to regulate the function of surrounding nerves. IGF-1 has consistently been of focus as a mediator of this relationship between muscle and motor neuron, as discussed previously as muscle-targeted therapy in ALS, a muscle-specific IGF-1 isoform administered to an SMBA mouse model delayed disease onset and improved survival by targeting the mutant AR protein via the Akt signalling pathway (Palazzolo et al., 2009).

Our findings that AR antagonism exacerbates the phenotype of male SOD1^{G93A} mice supports other studies manipulating androgens in this mouse model. Administration of DHT was shown to attenuate skeletal muscle atrophy, motor neuron degeneration and improve the clinical phenotype of SOD1^{G93A} mice, (Yoo & Ko, 2012) and this effect was attributed to elevated production of IGF-1 in muscle which provided neurotrophic support to motor neurons. The effect of DHT is in contrast to that of nandrolone, a synthetic anabolic steroid, which when given to castrated SOD1^{G93A} mice exacerbated disease onset and hastened death, in spite of hypertrophic effects on muscle (Aggarwal et al., 2014). The key difference between nandrolone and testosterone is their transcriptional gene targets with nandrolone having a myotrophic:androgenic ratio of ~11:1 compared to that of testosterone at ~1:1 (Kicman, 2008). Additionally, nandrolone suppresses the production of endogenous testosterone, therefore the potential of androgen therapies to modify ALS disease processes may be better focused on the enhancement of androgenic effects to motor neurons, rather than the anabolic effects in the muscle tissue alone.

In conclusion, the present study demonstrates for the first time that administration of an anti-androgen, flutamide, accelerates disease onset and motor deficits in male SOD1^{G93A} mice. As evidenced by exacerbated muscle wasting in symptomatic stages of disease, this is likely a reflection of peripherally-mediated effects where androgen receptor signalling is impacting secondary disease mechanisms. Our study is consistent with a role of androgens in modulating disease severity and sexual dimorphism in ALS.

718

CONFLICT OF INTEREST

The authors do not declare any conflict of interest.

Declaration of transparency and scientific rigour

This Declaration acknowledges that this paper adheres to the principles for transparent reporting and scientific rigour of preclinical research as stated in the *BJP* guidelines for Design & Analysis, Immunoblotting and Immunochemistry, and Animal Experimentation, and as recommended by funding agencies, publishers and other organisations engaged with supporting research.

ACKNOWLEDGMENTS

We thank Assoc. Prof. Clare Parish and Dr Jon Niclis for providing H9 cells and expertise on differentiations. Funding for this project was provided by the Australian NHMRC (Project Grants 1104295, 1104299), Stafford Fox Medical Research Foundation, MND Research Institute of Australia (Ted Dimmick Memorial MND Research Grant), Pratt Foundation and Mr Tony Gray. VM was supported by an MND Research Institute of Australia PhD Scholarship Top-Up Grant, BT was supported by an NHMRC-ARC Dementia Research Leadership Fellowship.

744 **REFERENCES**

745 Aare S, Spendiff S, Vuda M, Elkrief D, Perez A, Wu Q*, et al.* (2016). Failed reinnervation in aging skeletal
746 muscle. Skelet Muscle 6**:** 29.

747
748 Acsadi G, Anguelov RA, Yang H, Toth G, Thomas R, Jani A*, et al.* (2002). Increased survival and function of
749 SOD1 mice after glial cell-derived neurotrophic factor gene therapy. Hum Gene Ther 13**:** 1047-1059.

750
751 Aggarwal T, Polanco MJ, Scaramuzzino C, Rocchi A, Milioto C, Emionite L*, et al.* (2014). Androgens affect
752 muscle, motor neuron, and survival in a mouse model of SOD1-related amyotrophic lateral sclerosis.
753 Neurobiol Aging 35**:** 1929-1938.

754
755 Aizawa Y, Ikemoto I, Kishimoto K, Wada T, Yamazaki H, Ohishi Y*, et al.* (2003). Flutamide-induced hepatic
756 dysfunction in relation to steady-state plasma concentrations of flutamide and its metabolites. Mol Cell
757 Biochem 252**:** 149-156.

758
759 Alexander SP, Cidlowski JA, Kelly E, Marrion NV, Peters JA, Faccenda E*, et al.* (2017). THE CONCISE GUIDE
760 TO PHARMACOLOGY 2017/18: Nuclear hormone receptors. Br J Pharmacol 174 Suppl 1**:** S208-S224.

761
762 Asade RH, Prizont L, Muino JP, & Tessler J (1991). Steady-state hydroxyflutamide plasma levels after the
763 administration of two dosage forms of flutamide. Cancer Chemother Pharmacol 27**:** 401-405.

764
765 Azzouz M, Ralph GS, Storkebaum E, Walmsley LE, Mitrophanous KA, Kingsman SM*, et al.* (2004). VEGF
766 delivery with retrogradely transported lentivector prolongs survival in a mouse ALS model. Nature 429**:**
767 413-417.

768
769 Beitel LK, Alvarado C, Mokhtar S, Paliouras M, & Trifiro M (2013). Mechanisms mediating spinal and
770 bulbar muscular atrophy: investigations into polyglutamine-expanded androgen receptor function and
771 dysfunction. Front Neurol 4**:** 53.

772
773 Brown RH, Jr., & Al-Chalabi A (2017). Amyotrophic Lateral Sclerosis. N Engl J Med 377**:** 1602.

774
775 Cantor S, Zhang W, Delestree N, Remedio L, Mentis GZ, & Burden SJ (2018). Preserving neuromuscular
776 synapses in ALS by stimulating MuSK with a therapeutic agonist antibody. Elife 7.

777
778 Cary GA, & La Spada AR (2008). Androgen receptor function in motor neuron survival and degeneration.
779 Phys Med Rehabil Clin N Am 19**:** 479-494, viii.

780

781 Cortes CJ, & La Spada AR (2014). Motor neuron degeneration in spinal and Bulbar Muscular Atrophy is a
782 skeletal muscle-driven process: Relevance to therapy development and implications for related motor
783 neuron diseases. Rare Dis 2**:** e962402.

784
785 Cortes CJ, Ling SC, Guo LT, Hung G, Tsunemi T, Ly L*, et al.* (2014). Muscle expression of mutant androgen
786 receptor accounts for systemic and motor neuron disease phenotypes in spinal and bulbar muscular
787 atrophy. Neuron 82**:** 295-307.

788
789 Culig Z, Hoffmann J, Erdel M, Eder IE, Hobisch A, Hittmair A*, et al.* (1999). Switch from antagonist to
790 agonist of the androgen receptor bicalutamide is associated with prostate tumour progression in a new
791 model system. Br J Cancer 81**:** 242-251.

792
793 Curtis MJ, Bond RA, Spina D, Ahluwalia A, Alexander SP, Giembycz MA*, et al.* (2015). Experimental design
794 and analysis and their reporting: new guidance for publication in BJP. Br J Pharmacol 172**:** 3461-3471.

795
796 Da Cruz S, Parone PA, Lopes VS, Lillo C, McAlonis-Downes M, Lee SK*, et al.* (2012). Elevated PGC-1alpha
797 activity sustains mitochondrial biogenesis and muscle function without extending survival in a mouse
798 model of inherited ALS. Cell Metab 15**:** 778-786.

799
800 Dobrowolny G, Aucello M, Rizzuto E, Beccafico S, Mammucari C, Boncompagni S*, et al.* (2008). Skeletal
801 muscle is a primary target of SOD1G93A-mediated toxicity. Cell Metab 8**:** 425-436.

802
803 Dobrowolny G, Bernardini C, Martini M, Baranzini M, Barba M, & Musaro A (2015). Muscle Expression of
804 SOD1(G93A) Modulates microRNA and mRNA Transcription Pattern Associated with the Myelination
805 Process in the Spinal Cord of Transgenic Mice. Front Cell Neurosci 9**:** 463.

806
807 Dobrowolny G, Giacinti C, Pelosi L, Nicoletti C, Winn N, Barberi L*, et al.* (2005). Muscle expression of a
808 local Igf-1 isoform protects motor neurons in an ALS mouse model. J Cell Biol 168**:** 193-199.

809
810 Du ZW, Chen H, Liu H, Lu J, Qian K, Huang CL*, et al.* (2015). Generation and expansion of highly pure
811 motor neuron progenitors from human pluripotent stem cells. Nat Commun 6**:** 6626.

812
813 Fargo KN, Galbiati M, Foecking EM, Poletti A, & Jones KJ (2008). Androgen regulation of axon growth
814 and neurite extension in motoneurons. Horm Behav 53**:** 716-728.

815
816 Frey D, Schneider C, Xu L, Borg J, Spooren W, & Caroni P (2000). Early and selective loss of
817 neuromuscular synapse subtypes with low sprouting competence in motoneuron diseases. J Neurosci
818 20**:** 2534-2542.

819

Galbiati M, Onesto E, Zito A, Crippa V, Rusmini P, Mariotti R*, et al.* (2012). The anabolic/androgenic steroid nandrolone exacerbates gene expression modifications induced by mutant SOD1 in muscles of mice models of amyotrophic lateral sclerosis. Pharmacol Res 65**:** 221-230.

Gao W, Bohl CE, & Dalton JT (2005). Chemistry and structural biology of androgen receptor. Chem Rev 105**:** 3352-3370.

Geevasinga N, Menon P, Ozdinler PH, Kiernan MC, & Vucic S (2016). Pathophysiological and diagnostic implications of cortical dysfunction in ALS. Nat Rev Neurol 12**:** 651-661.

Harding SD, Sharman JL, Faccenda E, Southan C, Pawson AJ, Ireland S*, et al.* (2018). The IUPHAR/BPS Guide to PHARMACOLOGY in 2018: updates and expansion to encompass the new guide to IMMUNOPHARMACOLOGY. Nucleic Acids Res 46**:** D1091-D1106.

Holzbaur EL, Howland DS, Weber N, Wallace K, She Y, Kwak S*, et al.* (2006). Myostatin inhibition slows muscle atrophy in rodent models of amyotrophic lateral sclerosis. Neurobiol Dis 23**:** 697-707.

Kaspar BK, Llado J, Sherkat N, Rothstein JD, & Gage FH (2003). Retrograde viral delivery of IGF-1 prolongs survival in a mouse ALS model. Science 301**:** 839-842.

Katsuno M, Adachi H, Doyu M, Minamiyama M, Sang C, Kobayashi Y*, et al.* (2003). Leuprorelin rescues polyglutamine-dependent phenotypes in a transgenic mouse model of spinal and bulbar muscular atrophy. Nat Med 9**:** 768-773.

Kicman AT (2008). Pharmacology of anabolic steroids. Br J Pharmacol 154**:** 502-521.

Kujawa KA, Emeric E, & Jones KJ (1991). Testosterone differentially regulates the regenerative properties of injured hamster facial motoneurons. J Neurosci 11**:** 3898-3906.

La Spada AR, Wilson EM, Lubahn DB, Harding AE, & Fischbeck KH (1991). Androgen receptor gene mutations in X-linked spinal and bulbar muscular atrophy. Nature 352**:** 77-79.

Manzano R, Toivonen JM, Calvo AC, Olivan S, Zaragoza P, Rodellar C*, et al.* (2013). Altered in vitro proliferation of mouse SOD1-G93A skeletal muscle satellite cells. Neurodegener Dis 11**:** 153-164.

Manzano R, Toivonen JM, Olivan S, Calvo AC, Moreno-Igoa M, Munoz MJ*, et al.* (2011). Altered expression of myogenic regulatory factors in the mouse model of amyotrophic lateral sclerosis. Neurodegener Dis 8**:** 386-396.

Marchetti B, & Labrie F (1988). Characteristics of flutamide action on prostatic and testicular functions in the rat. J Steroid Biochem 29**:** 691-698.

Marron TU, Guerini V, Rusmini P, Sau D, Brevini TA, Martini L*, et al.* (2005). Androgen-induced neurite outgrowth is mediated by neuritin in motor neurones. J Neurochem 92**:** 10-20.

Matsuzaki Y, Nagai D, Ichimura E, Goda R, Tomura A, Doi M*, et al.* (2006). Metabolism and hepatic toxicity of flutamide in cytochrome P450 1A2 knockout SV129 mice. J Gastroenterol 41**:** 231-239.

McCombe PA, & Henderson RD (2010). Effects of gender in amyotrophic lateral sclerosis. Gend Med 7**:** 557-570.

McGrath JC, Drummond GB, McLachlan EM, Kilkenny C, & Wainwright CL (2010). Guidelines for reporting experiments involving animals: the ARRIVE guidelines. Br J Pharmacol 160**:** 1573-1576.

Messi ML, Clark HM, Prevette DM, Oppenheim RW, & Delbono O (2007). The lack of effect of specific overexpression of IGF-1 in the central nervous system or skeletal muscle on pathophysiology in the G93A SOD-1 mouse model of ALS. Exp Neurol 207**:** 52-63.

Miller TM, Kim SH, Yamanaka K, Hester M, Umapathi P, Arnson H*, et al.* (2006). Gene transfer demonstrates that muscle is not a primary target for non-cell-autonomous toxicity in familial amyotrophic lateral sclerosis. Proc Natl Acad Sci U S A 103**:** 19546-19551.

Moloney EB, de Winter F, & Verhaagen J (2014). ALS as a distal axonopathy: molecular mechanisms affecting neuromuscular junction stability in the presymptomatic stages of the disease. Front Neurosci 8**:** 252.

Murphy L, & O'Shaughnessy PJ (1991). Testicular steroidogenesis in the testicular feminized (Tfm) mouse: loss of 17 alpha-hydroxylase activity. J Endocrinol 131**:** 443-449.

Neri R (1989). Pharmacology and pharmacokinetics of flutamide. Urology 34**:** 19-21; discussion 46-56.

Palazzolo I, Stack C, Kong L, Musaro A, Adachi H, Katsuno M*, et al.* (2009). Overexpression of IGF-1 in muscle attenuates disease in a mouse model of spinal and bulbar muscular atrophy. Neuron 63**:** 316-328.

Perera ND, Sheean RK, Lau CL, Shin YS, Beart PM, Horne MK*, et al.* (2017). Rilmenidine promotes MTOR-independent autophagy in the mutant SOD1 mouse model of amyotrophic lateral sclerosis without slowing disease progression. Autophagy**:** 1-18.

Pfohl SR, Halicek MT, & Mitchell CS (2015). Characterization of the Contribution of Genetic Background and Gender to Disease Progression in the SOD1 G93A Mouse Model of Amyotrophic Lateral Sclerosis: A Meta-Analysis. J Neuromuscul Dis 2**:** 137-150.

Pi M, & Quarles LD (2012). GPRC6A regulates prostate cancer progression. Prostate 72**:** 399-409.

Pun S, Santos AF, Saxena S, Xu L, & Caroni P (2006). Selective vulnerability and pruning of phasic motoneuron axons in motoneuron disease alleviated by CNTF. Nat Neurosci 9**:** 408-419.

Rana K, Lee NK, Zajac JD, & MacLean HE (2014). Expression of androgen receptor target genes in skeletal muscle. Asian J Androl 16**:** 675-683.

Renier KJ, Troxell-Smith SM, Johansen JA, Katsuno M, Adachi H, Sobue G*, et al.* (2014). Antiandrogen flutamide protects male mice from androgen-dependent toxicity in three models of spinal bulbar muscular atrophy. Endocrinology 155**:** 2624-2634.

Rooney J, Fogh I, Westeneng HJ, Vajda A, McLaughlin R, Heverin M*, et al.* (2017). C9orf72 expansion differentially affects males with spinal onset amyotrophic lateral sclerosis. J Neurol Neurosurg Psychiatry 88**:** 281.

Schulz M, Schmoldt A, Donn F, & Becker H (1988). The pharmacokinetics of flutamide and its major metabolites after a single oral dose and during chronic treatment. Eur J Clin Pharmacol 34**:** 633-636.

Scott S, Kranz JE, Cole J, Lincecum JM, Thompson K, Kelly N*, et al.* (2008). Design, power, and interpretation of studies in the standard murine model of ALS. Amyotroph Lateral Scler 9**:** 4-15.

Sheean RK, Weston RH, Perera ND, D'Amico A, Nutt SL, & Turner BJ (2015). Effect of thymic stimulation of CD4+ T cell expansion on disease onset and progression in mutant SOD1 mice. J Neuroinflammation 12**:** 40.

Simeoni S, Mancini MA, Stenoien DL, Marcelli M, Weigel NL, Zanisi M*, et al.* (2000). Motoneuronal cell death is not correlated with aggregate formation of androgen receptors containing an elongated polyglutamine tract. Hum Mol Genet 9**:** 133-144.

Sinha-Hikim I, Taylor WE, Gonzalez-Cadavid NF, Zheng W, & Bhasin S (2004). Androgen receptor in human skeletal muscle and cultured muscle satellite cells: up-regulation by androgen treatment. J Clin Endocrinol Metab 89**:** 5245-5255.

Taylor JP, Brown RH, Jr., & Cleveland DW (2016). Decoding ALS: from genes to mechanism. Nature 539**:** 197-206.

Tevell A, Lennernas H, Jonsson M, Norlin M, Lennernas B, Bondesson U*, et al.* (2006). Flutamide metabolism in four different species in vitro and identification of flutamide metabolites in human patient urine by high performance liquid chromatography/tandem mass spectrometry. Drug Metab Dispos 34**:** 984-992.

Thomson JA, Itskovitz-Eldor J, Shapiro SS, Waknitz MA, Swiergiel JJ, Marshall VS*, et al.* (1998). Embryonic stem cell lines derived from human blastocysts. Science 282**:** 1145-1147.

Towne C, Raoul C, Schneider BL, & Aebischer P (2008). Systemic AAV6 delivery mediating RNA interference against SOD1: neuromuscular transduction does not alter disease progression in fALS mice. Mol Ther 16**:** 1018-1025.

Tyagi S, Beqollari D, Lee CS, Walker LA, & Bannister RA (2017). Semi-automated Analysis of Mouse Skeletal Muscle Morphology and Fiber-type Composition. J Vis Exp.

van Roijen JH, Ooms MP, Weber RF, Brinkmann AO, Grootegoed JA, & Vreeburg JT (1997). Comparison of the response of rat testis and accessory sex organs to treatment with testosterone and the synthetic androgen methyltrienolone (R1881). J Androl 18**:** 51-61.

Vargas MR, Burton NC, Kutzke J, Gan L, Johnson DA, Schafer M*, et al.* (2013). Absence of Nrf2 or its selective overexpression in neurons and muscle does not affect survival in ALS-linked mutant hSOD1 mouse models. PLoS One 8**:** e56625.

Wang C, Liu Y, & Cao JM (2014). G protein-coupled receptors: extranuclear mediators for the non-genomic actions of steroids. Int J Mol Sci 15**:** 15412-15425.

Yoo YE, & Ko CP (2012). Dihydrotestosterone ameliorates degeneration in muscle, axons and motoneurons and improves motor function in amyotrophic lateral sclerosis model mice. PLoS One 7**:** e37258.

TABLES

Table 1. Primer sequences

Gene Name	Species	Forward Primer	Reverse Primer
Chat	Human	5'- TTTTGTGAGAGCCGTGACTG -3'	5'- GTCAATGGCCATCCCTGTTA -3'
Isl1	Human	5'- CGCCTTGCAGAGTGACATAG -3'	5'- AGGACTGGCTACCATGCTGT -3'
Mnx1	Human	5'- GCACCAGTTCAAGCTCAACA -3'	5'- CTTTTTGCTGCGTTTCCATT -3'
Gapdh	Human	5'- CTGACTTCAACAGCGACACC -3'	5'- CCCTGTTGCTGTAGCCAAAT -3'
Tgfb1	Mouse	5'- TGCGCTTGCAGAGATTAAAA-3'	5'-CGTCAAAAGACAGCCACTCA-3'
Myog	Mouse	5'- CAGTGAATGCAACTCCCACA-3'	5'- CTGTCCACGATGGACGTAAG-3'
Myod1	Mouse	5'-TACAGTGGCGACTCAGATGC-3'	5'-TAGTAGGCGGTGTCGTAGCC-3'
Chrng (nAChRγ)	Mouse	5'-GCAGGCAGTATTGGAGAAGC-3'	5'-ACGAGCCATGAGGTTACAGG-3'
Ncam1	Mouse	5'- CAGCAGTGAACCGTATTGGA-3'	5'-TCTGGCTCATCAAACTGCAC-3'
Musk	Mouse	5'- CTACCCTCAGCCCGAGATTT-3'	5'-TGTCTTCCACGCTCAGAATG-3'
Hprt1	Mouse	5'- GATCAGTCAACGGGGGACAT-3'	5'- CATTTTGGGGCTGTACTGCTT-3'

992 **FIGURE LEGENDS**

993 **Figure 1. Agonist and antagonist dose-responses of the luciferase AR reporter assay in human**
994 **embryonic stem cell-derived motor neurons.** qRT-PCR analysis of (A) ChAT, (B) ISL1 and (C) MNX1/HB9
995 expression various stages of the differentiation (stages 1-4) compared to undifferentiated cells at day 0.
996 (D) Western blot confirming HB9 protein expression and AR expression in experimental motor neurons
997 in the presence or absence of 10μM DHT. (E) Immunocytochemistry confirming the expression of
998 mature neuronal (TUJ1 and SMI-32) and motor neuron-specific (ChAT and HB9) markers in experimental
999 motor neurons. Scale bar = 50 μm. (F) Expression of AR in motor neurons showing nuclear localisation in
1000 the presence of 10μM DHT. Scale bar = 50 μm. (G) AR activation following 16 h treatment with either
1001 testosterone, DHT, flutamide and HF over a 0.1-10^5 nM concentration range with the EC_{50} indicated
1002 where applicable. (H) AR activation following 16 h co-treatment with testosterone and increasing
1003 concentrations of antagonist with IC_{50} value indicated for HF. Green dotted line indicates the basal 50
1004 nM testosterone concentration. (I) AR activation following 16 h co-treatment with DHT and increasing
1005 concentrations of antagonist with IC_{50} value indicated for HF. Red dotted line indicates the basal 10 nM
1006 DHT concentration. Data are presented as mean ± SEM, n=3 independent experiments.
1007
1008 **Figure 2. Testosterone, flutamide and metabolite concentrations in plasma and spinal cord of male**
1009 **SOD1^{G93A} mice treated with either a placebo control or flutamide-releasing s.c. implant from postnatal**
1010 **day 60 (P60).** (A) Plasma testosterone levels in control and flutamide-treated male mice from pre-
1011 implant to endstage of disease (n=5-14 mice per group). * P<0.05, significantly different to control; two-
1012 way ANOVA with Fisher's LSD test. (B) Plasma flutamide, HF and Flu-1 levels in plasma of flutamide-
1013 treated male mice from 14 days post-implant (P74) to endstage of disease (n=5-10 mice per group).
1014 Blue lines indicate when a 21-day slow-release pellet was implanted. (C) Spinal cord testosterone,

flutamide, HF and Flu-1 drug levels after 14 days post-treatment (P74) in male and female mice (n=5 mice per group). Data represent mean ± SEM.

Figure 3. Effect of chronic flutamide treatment on the weights of male sex organs in SOD1^{G93A} mice. (A) Representative images of seminal vesicles at postnatal day 120 (P120). (B) Seminal vesicle weights at P74 and P120. * P<0.05 significantly different from control; two-way ANOVA with Fisher's LSD test. (C) Prostate weights. * P<0.05 significantly different from control; two-way ANOVA with Fisher's LSD test. (D) Testis weights. Data represent mean ± SEM, n=5 mice per group.

Figure 4. AR protein expression levels and cellular distribution in skeletal muscle and spinal cord from control and flutamide treated male and female SOD1^{G93A} mice. (A) Immunoblot analysis of AR in gastrocnemius muscle relative to total protein levels at postnatal day 74 (P74) and (C) P120. Quantification of AR levels relative to male control group is shown for (B) P74 and (D) P120. # P<0.05, significantly different to male counterpart; two-way ANOVA with Fisher's LSD test comparing sex effect. (E) Immunoblot analysis of AR in spinal cord relative to total protein at P74 and (G) P120. Quantification of AR levels relative to male control group is shown for (F) P74 and (H) P120. # P<0.05, significantly different to male counterpart; two-way ANOVA with Fisher's LSD test comparing sex. *P<0.05, significantly different to male control; two-way ANOVA with Fisher's LSD test comparing treatments. (I) AR immunohistochemical analysis in gastrocnemius muscle of male mice at P120. AR-positive nuclei are indicated by arrowheads. Gastrocnemius myocyte nuclei were identified by positive Hoechst-labelling with quantification for (J) AR-positive nuclei and (K) total nuclei. *P<0.05 significantly different to control; Mann Whitney test. (L) AR immunohistochemical analysis of lumbar spinal cords of male mice at P120. Ventral horn motor neurons identified by ChAT immunolabelling with (M) quantification of AR-

positive nuclei in ChAT-positive motor neurons shown. Data represent mean ± SEM, n=5 mice per group. Scale bar = 50 µm.

Figure 5. Flutamide treatment accelerates disease onset and motor dysfunction in male SOD1^{G93A} mice. (A) Mean disease onset determined by body weight loss onset was significantly advanced in male mice receiving flutamide, compared to male control. * P<0.05, significantly different to control; # P<0.05, significantly different to male counterpart; two-way ANOVA with Fisher's LSD test comparing treatment and sex. (B) Rotarod function at the time of disease onset was significantly impaired in male mice treated with flutamide, compared to male controls. * P<0.05, significantly different to control; two-way ANOVA with Fisher's LSD test comparing treatment. (C, D) Kaplan-Meier curves of age at which mice showed onset of disease and (E, F) age to reach endstage of disease defined by hindlimb paralysis in flutamide and control male and female mice. Data represent mean ± SEM, n=10 mice per group.

Figure 6. Flutamide treatment aggravates hindlimb skeletal muscle atrophy in male SOD1^{G93A} mice. qRT-PCR analysis of (A) TGFβ1, (B) myogenin and (C) MyoD mRNA levels in gastrocnemius muscles of male mice at postnatal day 120 (P120). qRT-PCR analyses of (D) TGFβ1, (E) myogenin and (F) MyoD mRNA levels in gastrocnemius muscles of female mice at P120. * P<0.05 statistically significant to control, Student's t-test or Mann Whitney test where unequal variance indicated. (G) Photomicrograph of gastrocnemius muscle cross-sections with laminin immunohistochemistry. Scale bar = 100 µm. Quantification of (H) fibre number per unit of area (I) mean cross-sectional area (CSA) of measured fibres and (J) mean minimum ferret diameter of measured fibres. * P<0.05 significantly different to control, Student's t-test. (K) The distribution of measured fibre CSAs in flutamide treated males, compared to control treated. * P<0.05 significantly different to control, two-way ANOVA using repeated measures with Fisher's LSD test comparing treatment. Data represent mean ± SEM, n=5 mice per group.

Figure 7. Effect of flutamide treatment on hindlimb skeletal muscle denervation in male SOD1^{G93A} mice. qRT-PCR analysis of (A) nAChRγ, (B) NCAM1 and (C) MuSK mRNA levels in gastrocnemius muscle of flutamide and control treated mice at postnatal day 120 (P120). * P<0.05 significantly different to control; Student's t-test. (D) Histochemical staining of neuromuscular junctions (NMJ)s within the gastrocnemius muscle; postsynaptic motor end plates labelled with α-bungarotoxin (BTX) and immunolabelling of presynaptic nerves (NF) and nerve terminals (Syn). * denotes full innervation, † represents partial innervation and ‡ shows denervated end plates. Scale bar = 50 µm. (E) Quantification of innervated, partially denervated and fully denervated endplates (n=4 mice per group).

Figure 8. Effects of flutamide treatment on motor neuron and glial cell pathology in lumbar spinal cord ventral horns of SOD1^{G93A} mice at postnatal day 120 (P120). (A) Representative immunostaining of ChAT-positive motor neurons with (B) quantification. # P<0.05 significantly different to male counterpart; two-way ANOVA with Fisher's LSD test comparing sex effect. (C) Representative immunostaining of GFAP-positive astrocytes with (D) quantification of astrocytes. # P<0.05 significantly different to male counterpart; two-way ANOVA with Fisher's LSD test comparing sex effect. (E) Representative immunostaining of CD11b-positive microglia with (F) quantification of microglial cell counts. Data represent mean ± SEM, n=5 mice per group. Scale bars = 50 µm.

Figure 1

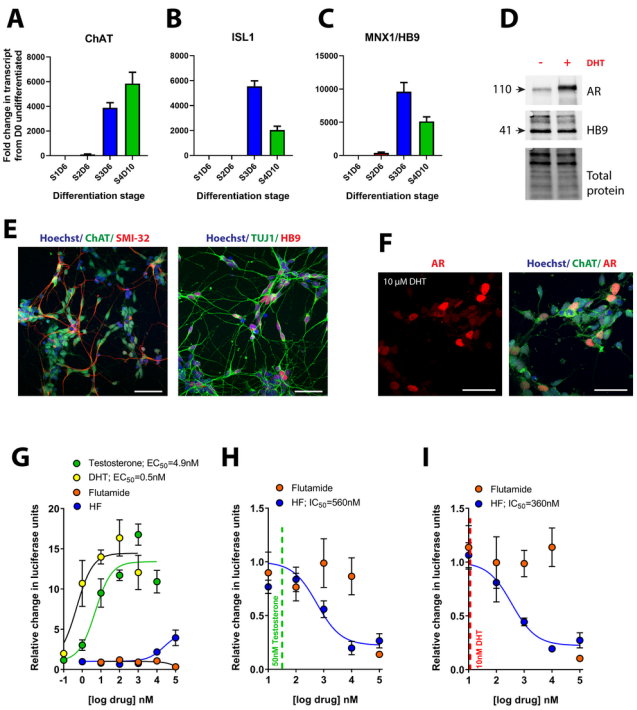

BPH_14657_Figure 1.tif

Figure 2

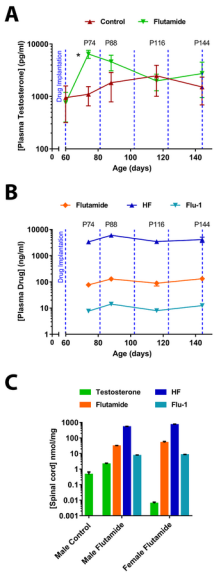

BPH_14657_Figure 2.tif

Figure 3

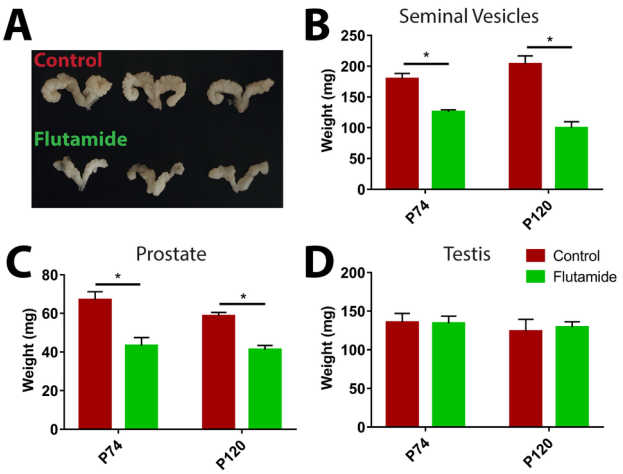

BPH_14657_Figure 3.tif

Figure 4

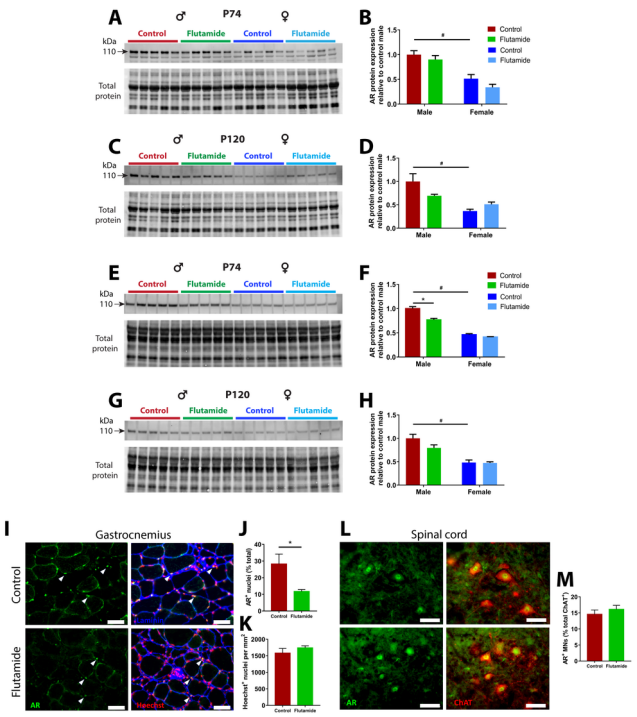

BPH_14657_Figure 4.tif

Figure 5

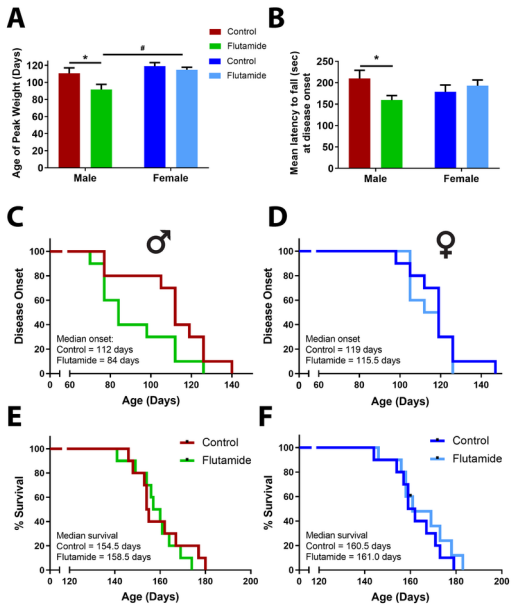

BPH_14657_Figure 5.tif

Figure 6

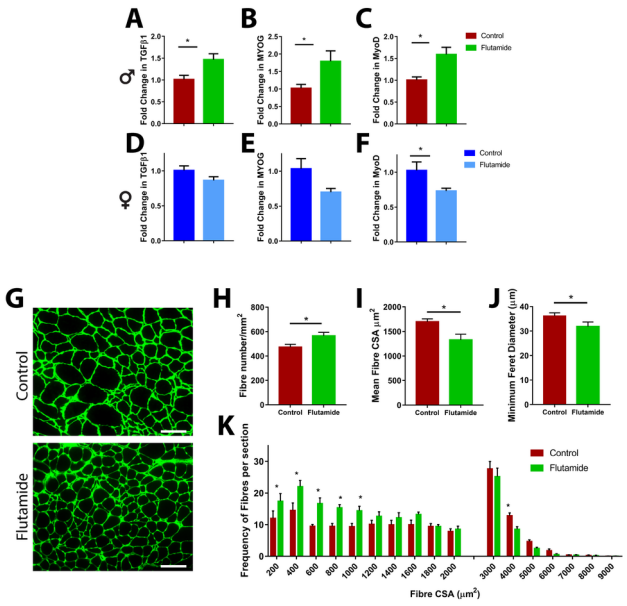

BPH_14657_Figure 6.tif

Figure 7

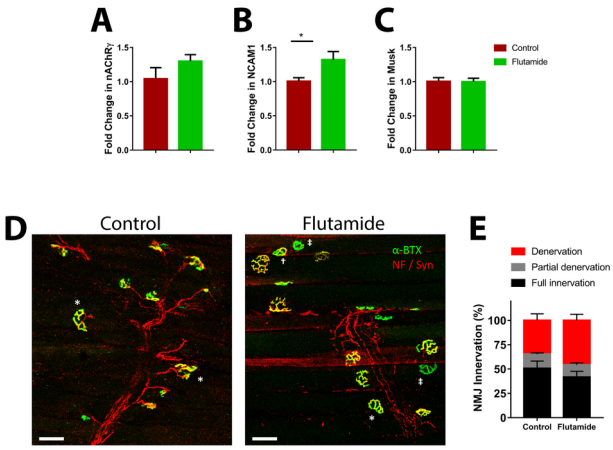

BPH_14657_Figure 7.tif

Figure 8

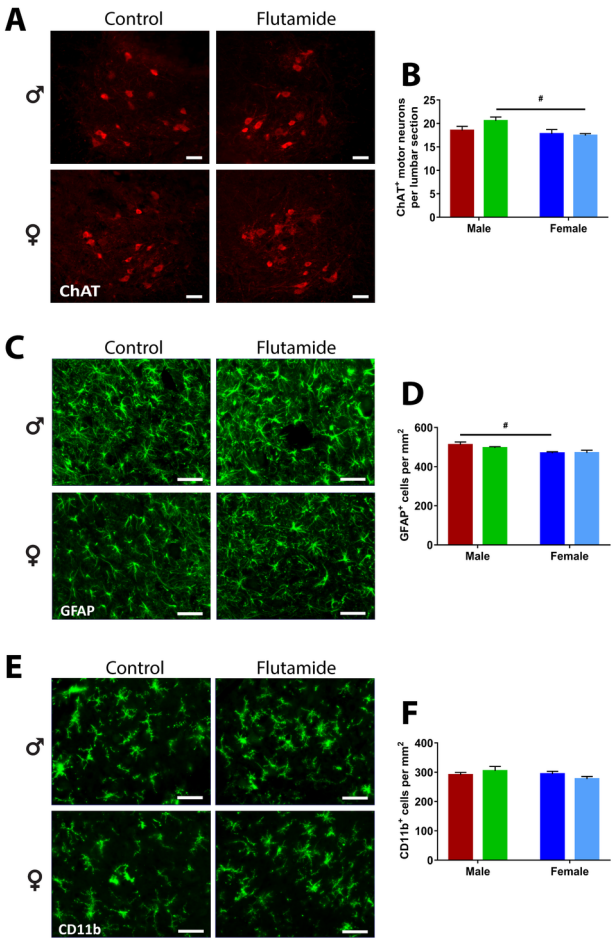

BPH_14657_Figure 8.tif